crystals

MDPI

Article

Temperature Stable, High-Quality Factor Li_2TiO_3-Li_4NbO_4F Microwave Dielectric Ceramics

Shangrui Xu [1], Juan Jiang [1,*], Zelai Cheng [1], Xiangyi Chen [1], Shikuan Sun [2], Dawei Wang [3,*] and Tianjin Zhang [1,*]

[1] School of Materials Science and Engineering, Hubei University, Wuhan 430062, China; xushangrui2021@163.com (S.X.); 17786125042@163.com (Z.C.); chen20xiangyi20@163.com (X.C.)
[2] School of Material Science and Energy Engineering, Foshan University, Foshan 528000, China; shikuansun@fosu.edu.cn
[3] Shenzhen Institute of Advanced Electronic Materials, Shenzhen Institute of Advanced Technology, Chinese Academy of Sciences, Shenzhen 518055, China
* Correspondence: jiangjuan@hubu.edu.cn (J.J.); wangdawei102@gmail.com (D.W.); zhangtj@hubu.edu.cn (T.Z.); Tel.: +86-13277085896 (J.J.); +86-13488651097 (D.W.); +86-13886122728 (T.Z.)

Abstract: In this work, (1-x)Li_2TiO_3-xLi_4NbO_4F ceramics were prepared by the conventional solid-state ceramic route. With the increase of Li_4NbO_4F content, the phase structure transformed from ordered monoclinic to disordered cubic. By increasing Li_3NbO_4F content, the temperature coefficient of resonant frequency (τ_f) was successfully adjusted closer to zero, while the dielectric constant (ε_r) and microwave quality factor (Q*f*) decreased to some degree. Outstanding microwave dielectric properties with a ε_r = 18.7, Q*f* = 61,388 GHz (6.264 GHz), and τ_f = 0.9 ppm/°C were obtained for 0.9Li_2TiO_3-0.1Li_4NbO_4F ceramics sintered at 1050 °C for 2 h, which indicated that these ceramics are suitable for practical applications in the field of microwave substrates and components.

Keywords: microwave dielectric properties; quality factor; Li_2TiO_3; Li_4NbO_4F

Citation: Xu, S.; Jiang, J.; Cheng, Z.; Chen, X.; Sun, S.; Wang, D.; Zhang, T. Temperature Stable, High-Quality Factor Li_2TiO_3-Li_4NbO_4F Microwave Dielectric Ceramics. *Crystals* **2021**, *11*, 741. https://doi.org/10.3390/cryst11070741

Academic Editors: Shujun Zhang and Francisco M. Morales

Received: 30 April 2021
Accepted: 21 June 2021
Published: 25 June 2021

1. Introduction

With the rapid development of wireless and mobile communication, new microwave dielectric ceramics with a suitable dielectric constant (ε_r), high microwave quality factor values (Q*f*, low dielectric loss), and near-zero temperature coefficient of resonant frequency ($\tau_f \approx 0$ ppm/°C) are desired for microwave device applications [1–6]. Recently, lithium-based microwave dielectric ceramics with rock salt, such as Li_2TiO_3, Li_3NbO_4, Li_2WO_4, and Li_2CeO_3, have gained plenty of attention because of their relatively low sintering temperature and excellent dielectric properties [7–9]. Among these ceramics, Li_2TiO_3 ceramics sintered at 1300 °C for 2 h showed superior microwave dielectric properties with a ε_r of 22, Q*f* value of 63,500 GHz (8.6 GHz), and τ_f value of +20.3 ppm/°C [10]. However, its practical applications were hindered because of the high sintering temperature as well as the positive τ_f value. In a previous study, B_2O_3 was added to Li_2TiO_3-Li_3NbO_4 ceramics to decrease the sintering temperature, and the results showed that the sintering temperature was decreased to 900 °C with the deterioration of the Q*f* value to 44,000 GHz [11]. On the other hand, LiF, as a kind of sintering aid, was reported to successfully decrease the sintering temperature in several microwave dielectric ceramic systems [12–14]. As reported, Li_4NbO_4F with a high Q*f*, low sintering temperature, and negative τ_f was studied extensively [15]. Therefore, in this work, Li_4NbO_4F ceramics were implemented as a sintering aid to adjust the τ_f value and decrease the sintering temperature for Li_2TiO_3 ceramics. (1-x)Li_2TiO_3-xLi_4NbO_4F (x = 0.05, 0.10, 0.15, 0.20) ceramics, compared with non-lithium based ceramics [16–18], were investigated in order to reduce the sintering temperature and achieve a near-zero τ_f value as well as a high Q*f* value. Their outstanding properties made the widespread application in a satellite communication and global positioning system antenna possible to achieve [19]. The phase structure, microstructure,

and microwave dielectric properties of (1-x)Li_2TiO_3-xLi_4NbO_4F (x = 0.05, 0.10, 0.15, 0.20) were studied in detail.

2. Experimental Procedure

(1-x)Li_2TiO_3-xLi_4NbO_4F ceramics were prepared by a conventional solid-state route. TiO_2 (99.9%, Sinopharm, China), Li_2CO_3 (99%, Sinopharm, China), N_2O_5 (99.9%, Zibo Weijie, China), and LiF (98%, Sinopharm, China) powders were used as starting materials. Stoichiometric Li_2CO_3 and TiO_2 were mixed according to the formula of Li_2TiO_3 and milled with ZrO_2 balls in ethanol for 6 h. Then, the mixtures were dried and calcined at 800 °C for 2 h in air. At the same time, stoichiometric Li_2CO_3, N_2O_5, and LiF were mixed, milled, dried, and calcined at 700 °C for 2 h in air in another furnace. The obtained Li_2TiO_3 and Li_4NbO_4F powders were weighed according to the designed molar ratios, mixed with 30 mL ethanol, and milled by balls for 8 h, dried, and sieved. Subsequently, the powders were sieved through 60 mesh. Then, the powder (the particle size at a scale of 4–10 μm) was granulated with 5 wt% PVA as binder and uniaxially pressed into cylindrical disks under a pressure of 100 MPa. These samples were buried by mixed powder with the same composition and sintered at 1000–1125 °C for 2 h at a heating rate of 3 °C/min.

The bulk densities of the sintered ceramics were measured by Archimedes method. The crystal structure was analyzed using X-ray diffraction (XRD) with Cu K_α radiation (D8-Advanced, Bruker, Germany). The microstructures were observed by a scanning electron microscope (SEM) (JSM 6510LV, JEOL Japan). Microwave dielectric properties were measured using a network analyzer (E5071C, Agilent, USA) with $TE_{01\delta}$ resonant mode. The temperature coefficient of the resonant frequency (τ_f) was calculated with the following formula:

$$\tau_f = \frac{(f_{80} - f_{25})}{f_{25}(80 - 25)} \times 10^6 \quad (1)$$

where f_{80} and f_{25} were the resonant frequencies at 80 °C and 25 °C, respectively.

3. Results and Discussion

The XRD patterns of the (1-x)Li_2TiO_3-xLi_4NbO_4F ceramics sintered at 1050 °C for 2 h are shown in Figure 1. It is well known that the Li_2TiO_3 phase has three modifications: the metastable cubic phase α-Li_2TiO_3, ordered monoclinic phase β-Li_2TiO_3, and disordered cubic phase γ-Li_2TiO_3. The α-Li_2TiO_3 phase transforms to the monoclinic β-Li_2TiO_3 phase at 670 °C, after which the reversible transition of the β-Li_2TiO_3 phase to the γ-Li_2TiO_3 phase occurs at 1150–1215 °C [20,21]. With the increase of x, the intensity of peaks, which belonged to the monoclinic phase, decreased, and there were only peaks belonging to cubic phase in the composition x = 0.20. The intensity of the (002) supercell peak, which was considered to indicate the degree of long-range order [22], decreased with the increase of x and finally faded away. At x = 0.05, the (311) and (222) supercell peaks were observed with low intensity, which belonged to cubic phase. This phenomenon showed that a true solid solution did not exist at x = 0.05. With the increase of x, the intensity of (200) and (220) supercell peaks was conspicuously enhanced, while (002) supercell peak vanished, showing that the ordered monoclinic phase transformed to the disordered cubic phase and totally transformed to the cubic phase between x = 0.10 and x = 0.15, which was consistent with the data in Table 1.

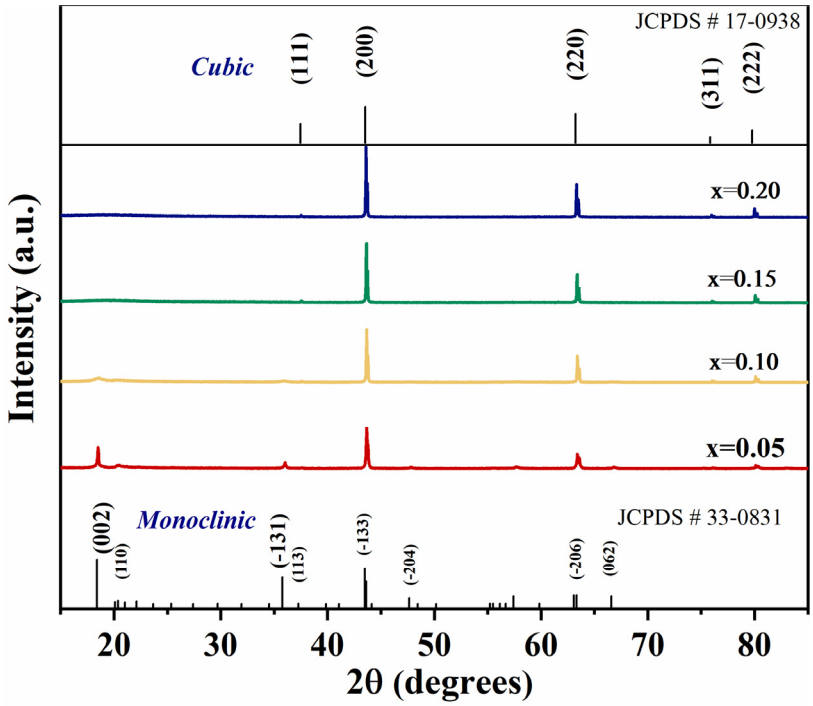

Figure 1. XRD patterns of (1-x)Li_2TiO_3-xLi_4NbO_4F ceramics sintered at 1050 °C for 2 h.

Table 1. Refinement parameters of (1-x)Li_2TiO_3-xLi_4NbO_4F ceramics sintered at 1050 °C for 2 h.

(1-x)Li_2TiO_3-xLi_4NbO_4F	Phase	a (Å)	a (Å)	a (Å)	α (°C)	β (°C)	γ (°C)	V (Å^3)	wt%	Rwp
x = 0.05	monoclinic cubic	5.07065 4.14846	8.77898 4.14846	9.76376 4.14846	90 90	100.0477 90	90 90	427.969 71.394	39.06 60.94	9.16
x = 0.10	monoclinic cubic	5.08391 4.14991	8.88845 4.14991	9.73513 4.14991	90 90	100.8609 90	90 90	432.032 71.468	27.00 73.00	10.5
x = 0.15	monoclinic cubic	4.15168	4.15168	4.15168	90	90	90	71.560	100.00	6.96
x = 0.20	monoclinic cubic	4.15476	4.15476	4.15476	90	90	90	71.720	100.00	6.18

To further demonstrate the phase transformation process, the XRD pattern was refined using the Fullprof software. The refinement results of the x = 0.10 sample are shown in Figure 2, and the lattice constants, R factors, and percentages of the phase for all the studied compositions are listed in Table 1. It was clear that the Li_2TiO_3 structure transformed from the ordered monoclinic phase to the disordered cubic phase with the increase of x. The ceramic unit cell volume with the cubic phase steadily increased from 71.394 Å^3 to 71.720 Å^3.

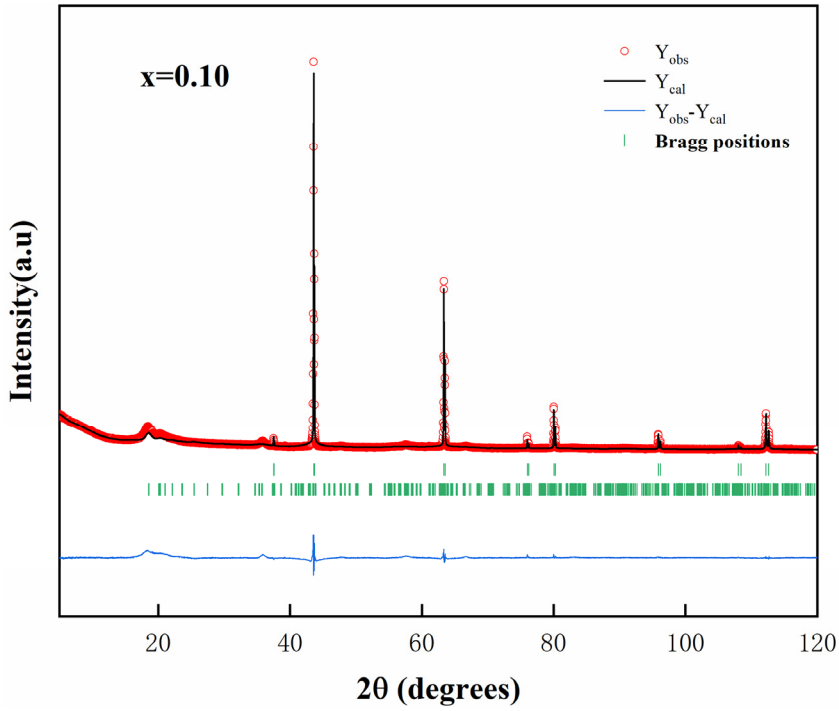

Figure 2. Refined XRD pattern of $0.90Li_2TiO_3$-$0.10Li_4NbO_4F$ ceramics sintered at 1050 °C for 2 h.

The SEM images of the (1-x)Li_2TiO_3-xLi_4NbO_4F ceramics sintered at 1050 °C are shown in Figure 3. All samples displayed porous microstructures, which were mainly attributed to the evaporation of lithium [23]. The porous microstructures were similar to those in pure Li_2TiO_3 ceramics, which indicated that it was difficult to improve the densification behavior of Li_2TiO_3 ceramics by adding Li_4NbO_4F [24]. Relatively small grains were observed for the compositions with x = 0.15 and 0.2, as shown in Figure 3c,d, which were likely due to the cubic phase grain, in agreement with the phase structure as shown in Figure 1 and Table 1.

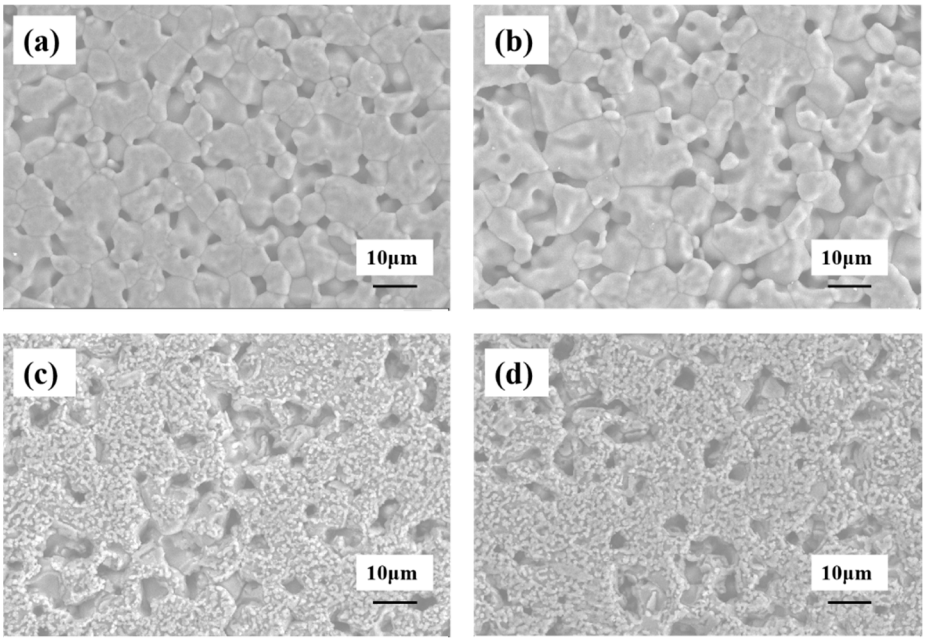

Figure 3. SEM micrographs of (1-x)Li_2TiO_3-xLi_4NbO_4F ceramics sintered at 1050 °C. (**a**) x = 0.05; (**b**) x = 0.10; (**c**) x = 0.15; (**d**) x = 0.20.

The EDS elemental mapping analysis of x = 0.05 and x = 0.20 for the ceramics sintered at 1050 °C for 2 h is given in Figures 4 and 5, respectively. It was obvious that F and Nb elements were heterogeneous in samples of x = 0.05, while elements were distributed homogeneously in samples of x = 0.20, which indicated that there were two phases of monoclinic and cubic phase coexistence in the sample of x = 0.05, whereas there was a one-phase solid solution in the sample of x = 0.20.

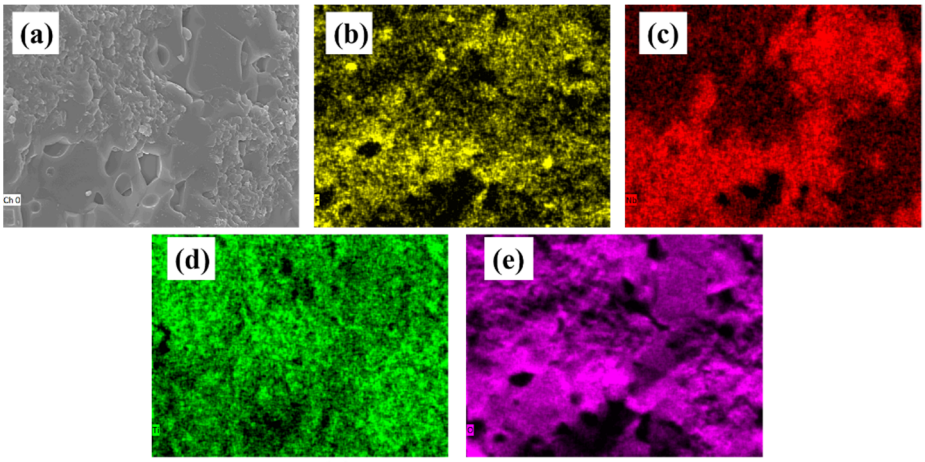

Figure 4. SEM micrographs (**a**) of $0.95Li_2TiO_3$-$0.05Li_4NbO_4F$ ceramics sintered at 1050 °C for 2 h and corresponding EDS analysis surface scanning of (**b**) F element, (**c**) Nb element, (**d**) Ti element, and (**e**) O element.

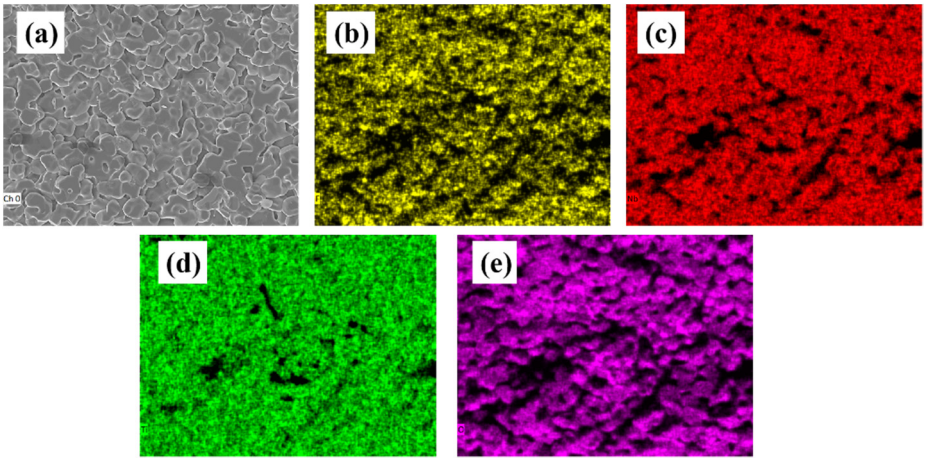

Figure 5. SEM micrographs (**a**) of $0.80Li_2TiO_3$-$0.20Li_4NbO_4F$ ceramics sintered at 1050 °C for 2 h and corresponding EDS analysis surface scanning of (**b**) F element, (**c**) Nb element, (**d**) Ti element, and (**e**) O element.

The bulk densities of ceramics with different Li_4NbO_4F content as a function of sintering temperature are presented in Figure 6. In the range of $x \leq 0.15$, with the increase of the sintering temperature, the bulk densities originally increased slightly but later obviously decreased at 1100 °C, which revealed that the ceramics had overburnt behavior when sintered at 1100 °C. These results agreed with more and more pores observed in Figure 3, but the bulk density of the ceramics at x = 0.20 increased with the increase of sintering temperature. On the other hand, as the x content increased, the density decreased.

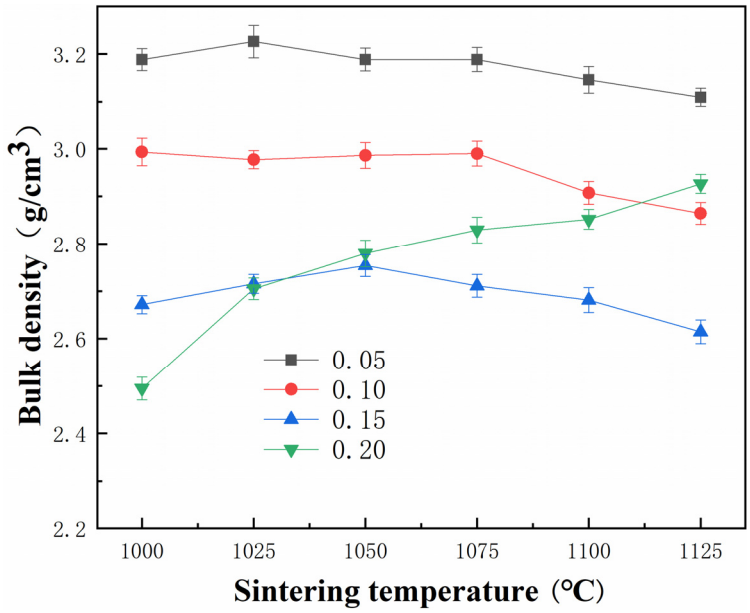

Figure 6. Variation of bulk density of (1-x)Li_2TiO_3-xLi_4NbO_4F ceramics sintered at 1000–1125 °C for 2 h.

Figure 7 displays the dielectric constant of samples sintered at various temperatures as a function of Li_4NbO_4F additions. With the increase of the sintering temperatures and Li_4NbO_4F content, the variations of ε_r coincided with bulk density, which suggested that the density was the main external factor that affected ε_r in the Li_2TiO_3-Li_4NbO_4F ceramics. It is well known that the ε_r of ceramics is mainly determined by the dipoles in the unit cell volume and the dielectric polarizabilities of ions [25]. A higher density means that are more dipoles in a unit volume. As shown in Figure 3, more and more pores were observed in the range of $x \leq 0.15$, which lowered the density and further influenced ε_r. In this case, with the exception of the composition, the ε_r of the Li_2TiO_3-Li_4NbO_4F samples was decided by bulk density, and the ε_r of the 0.90Li_2TiO_3-0.10Li_4NbO_4F ceramics was 18.7 with a near-zero τ_f value, which was suitable for the application of the integrated circuit.

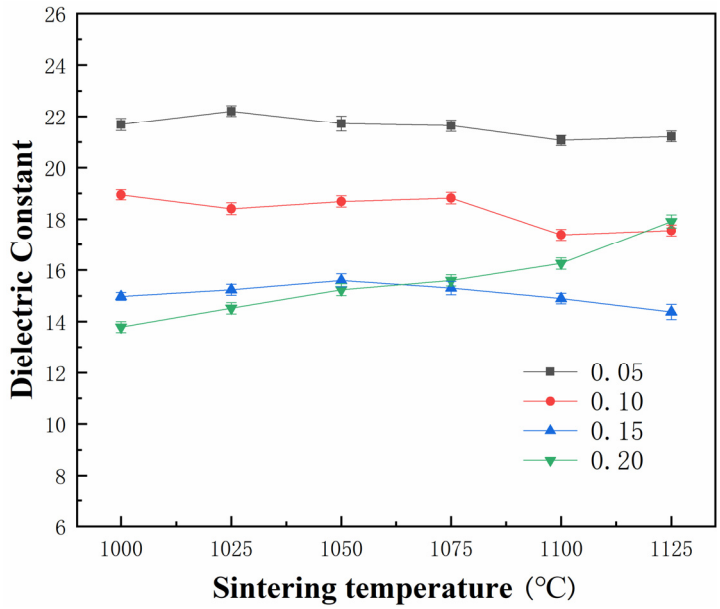

Figure 7. Dielectric constant of (1-x)Li_2TiO_3-xLi_4NbO_4F ceramics sintered at 1000–1125 °C for 2 h.

The variation of the Qf value of the (1-x)Li_2TiO_3-xLi_4NbO_4F ceramics with different sintering temperatures is plotted in Figure 8. The Qf values decreased with the increase of

Li_4NbO_4F content. The maximum *Qf* value of 76,202 GHz was achieved for the $0.95Li_2TiO_3$-$0.05Li_4NbO_4F$ ceramics sintered at 1100 °C. The desired ceramics with a near-zero τ_f and high *Qf* value of 61,388 GHz were acquired for the $0.90Li_2TiO_3$-$0.10Li_4NbO_4F$ ceramics sintered at 1050 °C, which was near to that of the pure Li_2TiO_3 (63,500 GHz). Compared with nonlithium-based ceramics, the Li_2TiO_3-Li_4NbO_4F ceramics and other lithium-based ceramics exhibited a relatively high *Qf* and low ε_r, as shown in Table 2. At x = 0.15 and x = 0.20, the *Qf* value increased linearly with the increase of the sintering temperature without the downward trend because the ceramics with the cubic phase need a higher sintering temperature than the ceramics with the monoclinic phase [26]. Microstructural defects, grain boundaries, porosity, and microcracks usually play important roles in dielectric loss [27]. As mentioned in Figure 3, more pores were observed in the $0.90Li_2TiO_3$-$0.10Li_4NbO_4F$ ceramics than in the $0.95Li_2TiO_3$-$0.05Li_4NbO_4F$ ceramics, which was consistent with the decrease of *Qf*.

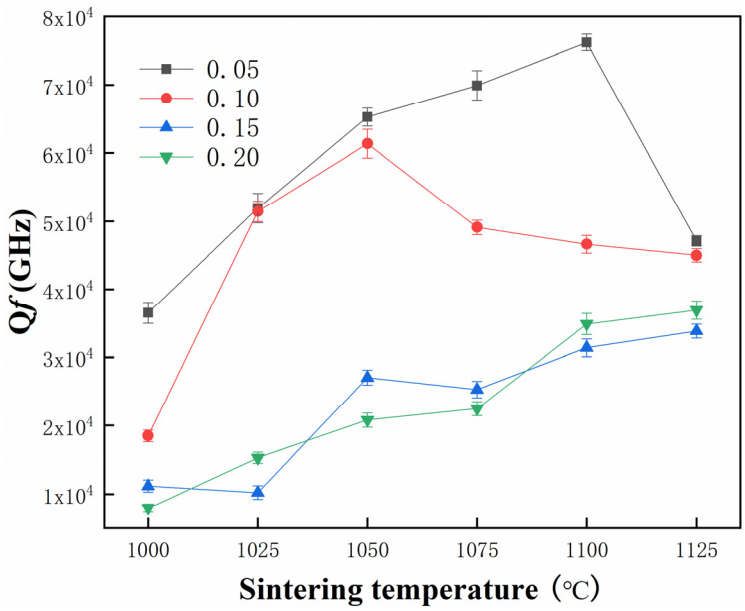

Figure 8. Quality factor of (1-x)Li_2TiO_3-xLi_4NbO_4F ceramics sintered at 1000–1125 °C for 2 h.

Table 2. Microwave dielectric properties of nonlithium and lithium-based microwave dielectric ceramics.

Material	ε_r	*Qf* (GHz)	τ_f (ppm/°C)	Sintering Temperature (°C)	Reference
$Ba_{1.85}Ca_{0.15}MgTi_5O_{13}$	29.3	30,870	+2.1	1160	[28]
$NiZrNb_2O_8$	23.77	40,280	−27.5	1200	[29]
$Ca_3Sn_{0.95}Ti_{0.05}Si_2O_9$	11.07	42,400	−5.1	1325	[30]
$ZnTiNb_2O_8$	35.5	52,500	−60	1050	[31]
$0.9Li_2TiO_3$-$0.1Li_4NbO_4F$	18.7	61,388	+0.9	1050	this work
Li_2TiGeO_5	9.43	65,300	+24.1	1140	[32]
$Li_3Mg_2SbO_6$	10.5	84,600	-9.0	1300	[33]
$Li_2Mg_{2.88}Ca_{0.12}TiO_6$	17.8	102,246	−0.7	1280	[34]

Figure 9 shows the variation of the τ_f value of the (1-x)Li_2TiO_3-xLi_4NbO_4F ceramics. τ_f was well known to be influenced by the composition, additive, and second phase of the materials [35]. With the increase of x, τ_f showed a negative trend. At x = 0.10, the $0.9Li_2TiO_3$-$0.1Li_4NbO_4F$ ceramics sintered at 1050 °C for 2 h achieved a τ_f of 0.9 ppm/°C, which is very important for applications.

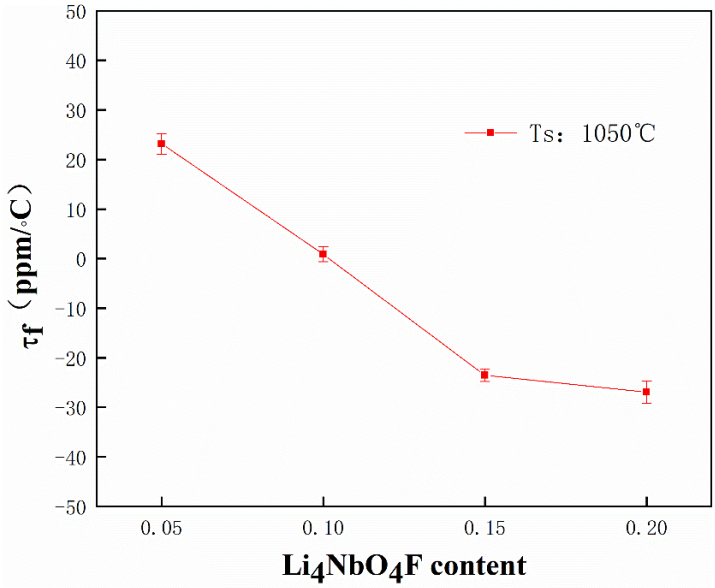

Figure 9. Temperature coefficient of resonant frequency of (1-x)Li_2TiO_3-xLi_4NbO_4F ceramics sintered at 1050 °C for 2 h.

4. Conclusions

In this work, the structural evolution, microstructure, surface analysis, and microwave dielectric properties of (1-x)Li_2TiO_3-xLi_4NbO_4F (x = 0.05, 0.10, 0.15, 0.20) ceramics have been investigated. Continuous solid solutions between Li_2TiO_3 and Li_4NbO_4F were formed across the entire compositional range, with the phase structure transforming from the monoclinic phase to cubic phase. With the increase of Li_4NbO_4F, the τ_f value of Li_2TiO_3-based ceramics was close to zero, and the sintering temperature of the ceramics was reduced. The Q*f* value of the Li_2TiO_3-xLi_4NbO_4F ceramics was conspicuously enhanced compared with that of the Li_2TiO_3-Li_3NbO_4 ceramics doped with B_2O_3. Excellent microwave dielectric properties of ε_r = 18.7, Q*f* = 61,388GHz, and τ_f = 0.9 ppm/°C were obtained for the 0.90Li_2TiO_3-0.10Li_4NbO_4F ceramics sintered at 1050 °C. The samples with a near-zero τ_f and high Q*f* were suitable for practical applications in the field of satellite communications and global positioning system antennas.

Author Contributions: Analysis and writing, S.X.; Review and editing, J.J. and D.W.; Methodology, S.S. and X.C.; Date curation, Z.C.; Project administration, T.Z. All authors have read and agreed to the published version of the manuscript.

Funding: This research was funded by the National Science Foundation of China (Grant Nos. 11774083 and 51902093) and China Scholarship Council (Grant No. 201808420353).

Conflicts of Interest: The authors declare no conflict and interest.

References

1. Wang, D.; Chen, J.; Wang, G.; Lu, Z.; Sun, S.; Li, J.; Jiang, J.; Zhou, D.; Song, K.; Reaney, I.M. Cold sintered $LiMgPO_4$ based composites for low temperature co-fired ceramic (LTCC) applications. *J. Am. Ceram. Soc.* **2020**, *103*, 6237–6244. [CrossRef]
2. Wang, D.; Siame, B.; Zhang, S.; Wang, G.; Ju, X.; Li, J.; Lu, Z.; Vardaxoglou, Y.; Whittow, W.; Cadman, D.; et al. Direct integration of cold sintered, temperature-stable $Bi_2Mo_2O_9$-K_2MoO_4 ceramics on printed circuit boards for satellite navigation antennas. *J. Eur. Ceram. Soc.* **2020**, *40*, 4029–4034. [CrossRef]
3. Wang, D.; Zhang, S.; Wang, G.; Vardaxoglou, Y.; Whittow, W.; Cadman, D.; Zhou, D.; Song, K.; Reaney, I.M. Cold sintered $CaTiO_3$-K_2MoO_4 microwave dielectric ceramics for integrated microstrip patch antennas. *Appl. Mater. Today* **2020**, *18*, 100519. [CrossRef]
4. Ratheesh, R.; Sebastian, M.T.; Mohanan, P.; Tobar, M.E.; Hartnett, J.; Woode, R.; Blair, D.G. Microwave characterization of $BaCe_2Ti_5O_{15}$ and $Ba_5Nb_4O_{15}$ ceramic dielectric resonators using whispering gallery mode method. *Mater. Lett.* **2000**, *45*, 279–285. [CrossRef]
5. Zhang, Q.L.; Yang, H.; Zou, J.L.; Wang, H.P. Sintering and microwave dielectric properties of LTCC-zinc titanate multilayers. *Mater. Lett.* **2005**, *59*, 880–884. [CrossRef]

6. Lei, W.; Lu, W.Z.; Zhu, J.H.; Wang, X.H. Microwave dielectric properties of $ZnAl_2O_4$–TiO_2 spinel-based composites. *Mater. Lett.* **2007**, *61*, 4066–4069. [CrossRef]
7. Liu, W.; Zuo, R. A novel Li_2TiO_3–Li_2CeO_3 ceramic composite with excellent microwave dielectric properties for low-temperature cofired ceramic applications. *J. Eur. Ceram. Soc.* **2018**, *38*, 119–123. [CrossRef]
8. Bian, J.; Liang, Z.; Wang, L. Structural evolution and microwave dielectric properties of $Li_{3-3x}M_{4x}Nb_{1-x}O_4$ (M = Mg, Zn; $0 \leq x \leq 0.9$). *J. Am. Ceram. Soc.* **2011**, *94*, 1447–1453. [CrossRef]
9. Zhou, D.; Wang, H.; Pang, L.-X.; Yao, X.; Wu, X.-G. Microwave dielectric characterization of a Li_3NbO_4 ceramic and its chemical compatibility with silver. *J. Am. Ceram. Soc.* **2008**, *91*, 4115–4117. [CrossRef]
10. Ding, Y.; Bian, J. Structural evolution, sintering behavior and microwave dielectric properties of $(1-x)Li_2TiO_3$+ xLiF ceramics. *Mater. Res. Bull.* **2013**, *48*, 2776–2781. [CrossRef]
11. Wang, F.; Yao, C.F.; Zeng, Q.; Zhou, H.; Zhou, Z.Y. *Structures, Dielectric Properties and Luminescence Properties of Nb Doped Li_2TiO_3 Solid Solution Ceramics//Key Engineering Materials*; Trans Tech Publications Ltd.: Freienbach, Switzerland, 2017; Volume 748, pp. 137–142.
12. Hao, Y.Z.; Yang, H.; Chen, G.H.; Zhang, Q.L. Microwave dielectric properties of Li_2TiO_3 ceramics doped with LiF for LTCC applications. *J. Alloy. Compd.* **2013**, *552*, 173–179. [CrossRef]
13. Xu, N.X.; Zhou, J.H.; Yang, H.; Zhang, Q.; Wang, M.; Hu, L. Structural evolution and microwave dielectric properties of MgO–LiF co-doped Li_2TiO_3 ceramics for LTCC applications. *Ceram. Int.* **2014**, *40*, 15191–15198. [CrossRef]
14. Zhang, J.; Yue, Z.; Luo, Y.; Zhang, X.; Li, L. Novel low-firing forsterite-based microwave dielectric for LTCC applications. *J. Am. Ceram. Soc.* **2016**, *99*, 1122–1124. [CrossRef]
15. Chu, X.; Jiang, J.; Wang, J.; Wu, Y.; Gan, L.; Zhang, T. A new high-Q× f Li_4NbO_4F microwave dielectric ceramic for LTCC applications. *Ceram. Int.* **2021**, *47*, 4344–4351. [CrossRef]
16. Lou, W.; Song, K.; Hussain, F.; Liu, B.; Bafrooei, H.B.; Lin, H.; Su, W.; Shi, F.; Wang, D. Bond characteristics and microwave dielectric properties of $(Li_{0.5}Ga_{0.5})^{2+}$ doped Mg2Al4Si5O18 ceramics. *Ceram. Int.* **2020**, *46*, 28631–28638. [CrossRef]
17. Tan, Z.; Song, K.; Bafrooei, H.B.; Liu, B.; Wu, J.; Xu, J.; Lin, H.; Wang, D. The effects of TiO_2 addition on microwave dielectric properties of $Y_3MgAl_3SiO_{12}$ ceramic for 5G application. *Ceram. Int.* **2020**, *46*, 15665–15669. [CrossRef]
18. Song, Z.; Song, K.; Liu, B.; Zheng, P.; Bafrooei, H.B.; Su, W.; Lin, H.; Shi, F.; Wang, D.; Reaney, I.M. Temperature-dependent dielectric and Raman spectra and microwave dielectric properties of gehlenite-type $Ca_2Al_2SiO_7$ ceramics. *Int. J. Appl. Ceram. Technol.* **2020**, *17*, 771–777. [CrossRef]
19. Narang, S.B.; Bahel, S. Low loss dielectric ceramics for microwave applications: A review. *J. Ceram. Process. Res.* **2010**, *11*, 316–321.
20. Izquierdo, G.; West, A.R. Phase equilibria in the system Li_2O-TiO_2. *Mater. Res. Bull.* **1980**, *15*, 1655–1660. [CrossRef]
21. Mikkelsen, J.C., Jr. Pseudobinary phase relations of $Li_2Ti_3O_7$. *J. Am. Ceram. Soc.* **1980**, *63*, 331–335. [CrossRef]
22. Castellanos, M.; West, A.R. Order-disorder phenomena in oxides with rock salt structures: The system Li_2TiO_3-MgO. *J. Mater. Sci.* **1979**, *14*, 450–454. [CrossRef]
23. Bian, J.J.; Dong, Y.F. New high Q*f* microwave dielectric ceramics with rock salt structures:$(1-x)Li_2TiO_3$+ xMgO system ($0 \leq x \leq 0.5$). *J. Eur. Ceram. Soc.* **2010**, *30*, 325–330. [CrossRef]
24. Bian, J.J.; Dong, Y.F. Sintering behavior, microstructure and microwave dielectric properties of Li_2+ $xTiO_3$ ($0 \leq x \leq 0.2$). *Mater. Sci. Eng. B* **2011**, *176*, 147–151. [CrossRef]
25. Sebastian, M.T. *Dielectric Materials for Wireless Communication*; Elsevier: Amsterdam, Netherlands, 2010.
26. Kleykamp, H. Phase equilibria in the Li–Ti–O system and physical properties of Li_2TiO_3. *Fusion Eng. Des.* **2002**, *61*, 361–366. [CrossRef]
27. Penn, S.J.; Alford, N.M.N.; Templeton, A.; Wang, X.; Xu, M.; Reece, M.; Schrapel, K. Effect of porosity and grain size on the microwave dielectric properties of sintered alumina. *J. Am. Ceram. Soc.* **1997**, *80*, 1885–1888. [CrossRef]
28. Dai, Q.; Zuo, R.; Xu, Y.; He, L. A novel temperature-stable $Ba_{2-x}Ca_xMgTi_5O_{13}$ microwave dielectric ceramic. *J. Eur. Ceram. Soc.* **2020**, *40*, 376–380. [CrossRef]
29. Xia, W.S.; Yang, F.Y.; Zhang, G.Y.; Han, K.; Guo, D.C. New low-dielectric-loss $NiZrNb_2O_8$ ceramics for microwave application. *J. Alloy. Compd.* **2016**, *656*, 470–475. [CrossRef]
30. Song, X.Q.; Du, K.; Zhang, X.Z.; Li, J.; Lu, W.Z.; Wang, X.C.; Lei, W. Crystal structure, phase composition and microwave dielectric properties of $Ca_3MSi_2O_9$ ceramics. *J. Alloy. Compd.* **2018**, *750*, 996–1002. [CrossRef]
31. Bafrooei, H.B.; Feizpour, M.; Sayyadi-Shahraki, A.; Song, K.X. High-performance $ZnTiNb_2O_8$ microwave dielectric ceramics produced from $ZnNb_2O_6$–TiO_2 nano powders. *J. Alloy. Compd.* **2020**, *834*, 155082. [CrossRef]
32. Cheng, K.; Tang, Y.; Xiang, H.; Li, C.; Fang, L.; Sun, Y. Two novel low permittivity microwave dielectric ceramics Li_2TiMO_5 (M= Ge, Si) with abnormally positive τf. *J. Eur. Ceram. Soc.* **2019**, *39*, 2680–2684. [CrossRef]
33. Pei, C.; Hou, C.; Li, Y.; Yao, G.; Ren, Z.; Liu, P.; Zhang, H. A low εr and temperature-stable $Li_3Mg_2SbO_6$ microwave dielectric ceramics. *J. Alloy. Compd.* **2019**, *792*, 46–49. [CrossRef]
34. Fang, Z.; Tang, B.; Si, F.; Zhang, S. Temperature stable and high-Q microwave dielectric ceramics in the $Li_2Mg_3 - xCa_xTiO_6$ system (x = 0.00–0.18). *Ceram. Int.* **2017**, *43*, 1682–1687. [CrossRef]
35. Huang, C.L.; Liu, S.S. Low-loss microwave dielectrics in the $(Mg1-xZnx)_2TiO_4$ ceramics. *J. Am. Ceram. Soc.* **2008**, *91*, 3428–3430. [CrossRef]